



Influence of the Presence of an Interbedded Weak Clay Layer on Ultimate Bearing Capacity of Sandy Soil Using AFELA and MARS

Shivesh Tripathi · Van Qui Lai · Shreyansh Singh · Shipra Pathak · Ananya Srivastava · Suraparb Keawsawasvong · Vinay Bhushan Chauhan

Received: 11 October 2022 / Accepted: 7 February 2023 / Published online: 18 February 2023
© The Author(s), under exclusive licence to Springer Nature Switzerland AG 2023

Abstract In this study, the impact of the presence of a compressible clay layer on the ultimate bearing capacity (*UBC*) of a strip footing supported by a layered soil stratum is evaluated using Adaptive Finite Element Limit Analysis (*AFELA*). The normalized depth of the compressible layer (*H/B*), internal friction angle of the sandy soil (ϕ), and undrained shear strength of the clay layer (S_u) were varied as independent parameters over a range of 0.5 to 7, 30° to 45°, and 12 kPa to 192 kPa, respectively, in the computational analysis. The results stipulate that as the clay layer embeds deeper into the soil strata, the bearing capacity ratio (*BCR*) and the settlement of the footing increase. The location of the compressible layer has the maximum influence on the settlement of the footing, contrary to ϕ , and S_u , whose influence is found to be relatively minor in the analysis. A data

science technique known as the ‘Multivariate Adaptive Regression Spline’ (*MARS*) has been adopted to develop an empirical equation that represents the relationship between the ultimate bearing capacity (*UBC*) of a strip footing on a layered soil stratum and the input parameters. The R^2 value of the empirical equation is found to be 0.9942, indicating a high degree of accuracy in predicting the *UBC*. Additionally, a sensitivity analysis using *MARS* is performed to determine the relative importance of each input parameter in affecting the *UBC*.

Keywords Adaptive finite element limit analysis · Bearing capacity · MARS · Compressible layer · Mohr-Coulomb · Tresca failure criterion

S. Tripathi · S. Singh · S. Pathak
Civil Engineering Department, Madan
Mohan Malaviya University of Technology,
Gorakhpur, Uttar Pradesh 273010, India

V. Q. Lai
Faculty of Civil Engineering, Ho Chi Minh City University
of Technology (HCMUT), 268 Ly Thuong Kiet Street,
District 10, Ho Chi Minh City, Vietnam
e-mail: lvqui@hcmut.edu

V. Q. Lai
Vietnam National University Ho Chi Minh City
(VNU-HCM), Linh Trung Ward, Thu Duc District,
Ho Chi Minh City, Vietnam

A. Srivastava
Department of Civil and Infrastructure Engineering,
Indian Institute of Technology Jodhpur, Jodhpur,
Rajasthan 342030, India
e-mail: ananyashri.work@gmail.com

S. Keawsawasvong
Department of Civil Engineering, Thammasat School
of Engineering, Thammasat University, Pathumthani,
Thailand
e-mail: ksurapar@engr.tu.ac.th

V. B. Chauhan (✉)
Civil Engineering Department, Madan
Mohan Malaviya University of Technology,
Gorakhpur, Uttar Pradesh 273010, India
e-mail: vbce@mmmut.ac.in; chauhan.vinaybhushan@gmail.com

1 Introduction

The fast growth of industrialization globally has made it difficult to find adequate land for secure construction, as suitable land has become scarce. Currently, finding firm ground for a building is a significant challenge. Consequently, due to the aforementioned reasons, the utilization of soft or weak soil masses with inadequate bearing capacity is now being executed after undergoing necessary modifications. Several studies have used a variety of approaches to increase the bearing capability of the soil when a footing is placed at the top of a weak soil stratum. The technique removes the soft soil already present up to a shallow depth and replaces it with granular soil with horizontal reinforcement layers. Additionally, the ground substituted with reinforced soil could be compacted at a higher density to gain the advantage of more frictional resistance. If the removed soil is very loose, it might be altered with well-graded soil before being strengthened and re-compacted. Under such circumstances where a non-homogenous/stratified soil layer supports the superstructure, the bearing capacity assessment is essential as there are variations in the soil constituents within a section of the earth strata (Gupta et al. 2021).

Prior research has conducted comprehensive investigations into the load-bearing capacity of foundations on homogeneous soil deposits (Terzaghi 1943; Meyerhof 1963; Lai et al. 2022a). Moreover, researchers have examined the behavior of footings lying above the reinforced earth, including the assessment of the bearing capacity ratio (*BCR*) (i.e., the ratio of reinforced soils to unreinforced soil's ultimate bearing capacity) on shallow foundations (Meyerhof and Hanna 1978; Hanna and Meyerhof 1980; Akinmusuru and Akinbolade 1981; Fragaszy and Lawton 1984; Mandal and Sah 1992; Srinivasa et al. 1993; Jaiswal et al. 2021, Keawsawasvong et al. 2022a; Jaiswal et al. 2022a). A small-scale laboratory model test was conducted to compare and study the performance of granular fill overlays, with and without geogrid reinforcement, on a soft soil layer subjected to foundation load. The results of the test indicated a considerable enhancement in the ultimate bearing capacity ratio and a significant decrease in foundation settlement. Furthermore, Cicek and Guler (2015) calculated the ultimate carrying capacity of strip footings placed on geosynthetic reinforced sand soils by

the limit equilibrium method as well as the finite element method. The majority of studies have reported an increase in the load-bearing capacity of the underlying soil due to the incorporation of horizontal reinforcement layers. Nevertheless, for in-situ installation of these reinforcement layers, the weak soil layer must be excavated to a shallow depth and then re-compacted after placing the reinforcement layers at the appropriate spacing.

The homogeneity of soil strata is an uncommon phenomenon in nature. The evaluation of multi-layered soil formations is carried out using a combination of experimental methods and analytical techniques, including limit equilibrium, limit analysis, and various numerical methods (Hanna 1987; Michalowski and Shi 1995; Dewaikar and Mohapatra 2003; Kumar and Sahoo 2013; Chakraborty and Kumar 2014a; Chakraborty and Kumar 2014b; Kumar and Chakraborty 2015; Ukritchon and Keawsawasvong 2020; Keawsawasvong et al. 2022b; Rai et al. 2022). Michalowski and Shi (1995) employed the kinematic approach of limit equilibrium analysis to assess the load-bearing capacity of footings supported on a two-layer soil system, with the results of the study being applicable only to a specific scenario where the footing was placed on a granular soil layer overlying a clay layer. Shiau et al. (2003) utilized finite element limit analysis to examine the load-bearing capacity of a sand layer placed on top of the clay layer, analyzing the impact of changes in the model's geometry and strength parameters. Ghazavi and Eghbali (2008) presented a simple analytical technique based on limit equilibrium to compute the load-bearing capacity of shallow footings on two-layer granular (sandy) soil formations. Despite previous studies on layered soil formations, a comprehensive understanding of the performance of structures constructed on such soil strata is still lacking. Thus, the objective of the current study is to examine the ultimate bearing capacity (*UBC*) of soil strata incorporating a weak, compressible clay layer, through the use of adaptive finite element limit analysis (*AFELA*). The layered soil strata are subjected to a gradually increasing uniformly distributed vertical load in the form of a footing. The numerical model is created by a finite element-based computational tool and limit analysis and multiplier elastoplastic analysis are performed to understand the variation in the *UBC* of the footing, the change in the failure patterns,

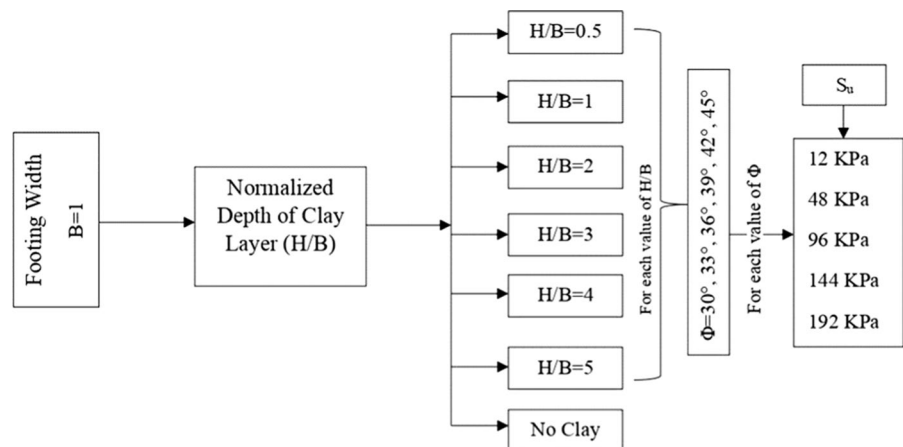
and the load-settlements behavior of the foundation due to the presence of a compressible clay layer. The governing parameters for the computational analysis, namely the normalized depth of the compressible layer (H/B), internal angle of friction of cohesionless soil (ϕ), and undrained shear strength (S_u), are varied between 0.5 to 7, 30° to 45° , and 12 kPa to 192 kPa, respectively (Ameratunga et al. 2016). A total of 210 numerical models are simulated to conduct a comprehensive examination of the ultimate bearing capacity (UBC) of the strip footing. The examination aims to determine the variation in the bearing capacity ratio (BCR), the potential failure mode of the footing, and the settlement of the footing. The nonlinearities and interactions between variables are identified using a data science technique called "Multivariate Adaptive Regression Spline" ($MARS$) and a proposed empirical equation is developed to estimate the UBC under the specified conditions. Furthermore, the impact of the input parameters (H/B , ϕ , S_u) on UBC is examined by the sensitivity analysis in the $MARS$ model.

1.1 Problem Statement

The current study intends to evaluate BCR for different combinations of (ϕ) and (S_u) as shown in Fig. 1.

For the aforementioned, a two-dimensional finite element-based numerical computational tool, Optum G2 (2020), is used to model a strip footing, resting on a sand bed containing a compressible layer of clay. The normalized depth of the clay layer (H/B) is varied as $H/B = 0.5, 1, 2, 3, 4, 5$. Consequently, the study assesses the influence of H/B , ϕ and S_u on the settlement of the foundation and the extent of the failure

Fig. 1 Flowchart describing various parameters considered for the present analysis



plane beneath it, in addition to the assessment of the BCR of the footing on the layered soil. With this large number of presented results and the $MARS$ model, the findings shall be beneficial for the geotechnical engineers to design a safer structure resting on soil strata containing a weak clay layer.

2 Numerical Modeling

Figure 2 illustrates the typical arrangement of the layered soil strata for the numerical simulations considered in the present study. A detailed stratified soil system with geometrical configuration is shown in Fig. 2.

Here, a weightless and rigid strip footing of width, B (1m) is placed on the layered soil system, which is subjected to a uniformly distributed load. A clay layer of 1m thickness is sandwiched in between the

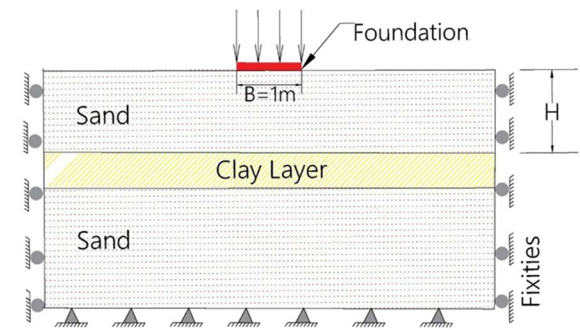


Fig. 2 Geometrical representation of the layered soil strata considered in the present study with load and boundary conditions

sand layers in the layered soil system. The distance between the clay layer from the bottom of the footing surface is represented by H . The abovementioned distance is normalized with the width of footing and represented as the normalized depth of the clay layer, H/B . The internal friction angle of the sand layer and the undrained shear strength of clay are represented by the ϕ and S_u , respectively. The sand layer is assumed to follow the Mohr-Coulomb failure criterion, whereas the clay layer follows the Tresca failure criterion. To present the noted results, a dimensionless bearing capacity ratio (BCR) is evaluated, which is defined as the ratio of the ultimate bearing capacity of the layered soil to the ultimate bearing capacity of homogenous sand strata.

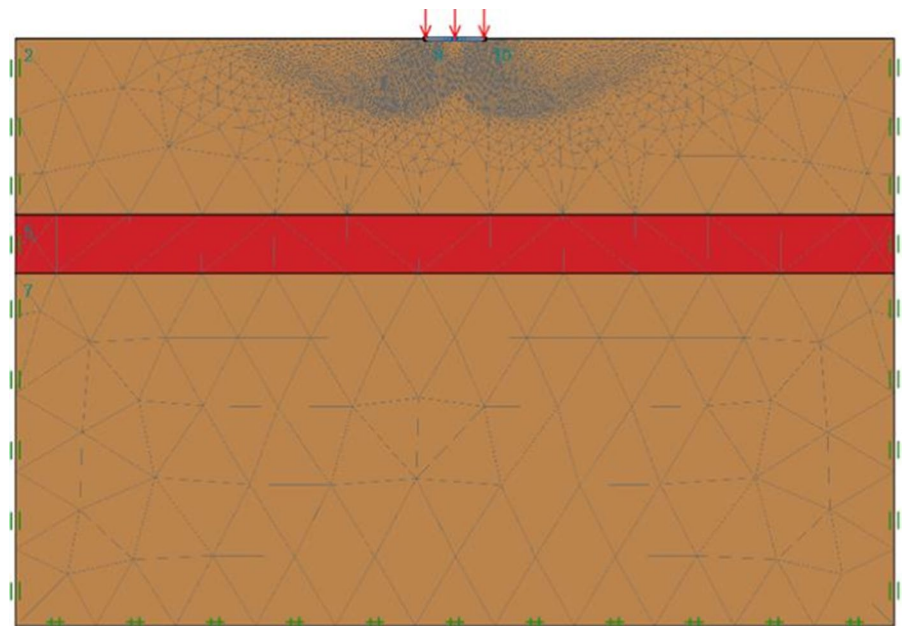
$$BCR = \frac{\text{Ultimate bearing capacity of layered soil}}{\text{Ultimate bearing capacity of homogenous sand strata}} \quad (1)$$

Figure 3 illustrates the finite element model of a compressible clay layer sandwiched between two sandy soil strata. The dimensions of the soil strata are 10m in depth and 15m in width. The normalized depth of the clay layer (H/B) is varied along with other engineering properties of sand and clay. The boundary conditions are established with standard fixities, where the bottom boundary is restrained from movement in all directions and the vertical

boundaries are restrained horizontally (Jaiswal and Chauhan 2021a, b). The boundaries of the finite element model are positioned away from the predicted failure zones to minimize any impact on the shear failure patterns and settlement behavior of the sand and clay layers (Jaiswal and Chauhan 2021c, d).

In numerical analysis, the size of the mesh element plays a vital role as the optimum average mesh size and the number of elements are evaluated to increase the accuracy of calculating stresses and minimize errors (Keawsawasvong and Ukritchon 2019; Ukritchon and Keawsawasvong 2019; Ukritchon et al. 2019; Keawsawasvong and Ukritchon 2020; Ukritchon et al. 2020; Keawsawasvong and Lai 2021; Yodsomjai et al. 2021; Lai et al. 2022b, 2022c; Keawsawasvong et al. 2022c). In the numerical analysis, the mesh element size is a crucial factor. To achieve an optimal average mesh size and the appropriate number of elements, the aim is to enhance the accuracy in the calculation of stresses while minimizing errors. The accuracy of the results is ensured by conducting a sensitivity analysis, in which the number of mesh elements is varied from 5000 to 20000 (Srivastava and Chauhan 2020; Chauhan et al. 2022). It is concluded that using more than 10,000 elements in the mesh ensures stability in the results with only negligible variations. Therefore, the optimum number of elements for the models used in the current study is

Fig. 3 Finite element model showing a strip footing resting on layered sand with the presence of a compressible clay layer



determined to be 10,000 (Jaiswal et al. 2022b; Ojha et al. 2021; Banyong and Keawsawasvong 2022). Sloan (2013) stated that the stability analysis using the *AFELA* based on the limit analysis theory requires only the conventional strength parameters such as cohesion and friction angle but does not require the deformation parameters such as Poisson's ratio and Young's modulus. Therefore, *FELA* differs from the conventional displacement-based finite element analysis. However, for the parameters mentioned earlier, a multiplier elastoplastic analysis has also been performed in order to analyze the load-settlement behavior of the footing.

3 Results and Discussion

This section provides a summary and discussion of the key findings obtained through numerical simulations. The results, depicted in graphical forms, assess the bearing capacity ratio (*BCR*) of the strip footing with variations in the governing parameters. Further analysis of the load-settlement curves and shear failure patterns of the various cases is conducted and discussed in subsequent sections.

3.1 Effect of H/B on *BCR*

Figure 4 shows the variation of *BCR* for varying H/B for the considered range of ϕ and S_u . For a clay layer situated near the ground level, i.e., $H/B = 0.5$, the highest *BCR* is obtained at $S_u = 192$ kPa and the lowest value of *BCR* is obtained at $S_u = 12$ kPa. Throughout the variation of S_u , the bearing capacity ratio of the footing decreases by 81.25% of its original value. Thus, it can be stated that the *BCR* of the strip footing is directly proportional to the S_u when the compressible layer is situated close to the foundation. However, the effect of ϕ , is considerably different on the *BCR*. The greatest value of *BCR* is obtained when the clay layer is sandwiched in sandy soil having a lower friction angle, i.e., $\phi = 33^\circ$ and the minimum when the sandy soil has a higher friction angle, i.e., $\phi = 45^\circ$. The *BCR* decreases by 62.5% as the value of ϕ is increased from 33° to 45° . Similarly for $H/B = 1$, the highest *BCR* is obtained at $S_u = 192$ kPa and the lowest value of *BCR* is obtained at $S_u = 12$ kPa with the bearing capacity ratio of the footing being decreased by 76% from the highest value. The highest value of

BCR, in this case, is gained at $\phi = 33^\circ$ and the lowest at $\phi = 45^\circ$ where the *BCR* decreases by 28.57% as the value of ϕ is increased. For $H/B = 2$ and 3, it is observed that the highest magnitude of *BCR* is 1.0 in all the cases, which gets lower due to the effect of S_u and ϕ . For $H/B = 4$ and 5, no effect of S_u and ϕ is at all observed and the *BCR* is constant at 1.0 except for the lowermost value of S_u (very soft clay) and the highest value of ϕ , considered in the study. Thus, apart from the cases of the extremum, the *BCR* is invariable, as if the presence of the clay layer does not affect the ultimate bearing capacity of the layered soil strata.

3.2 Effect of S_u on *BCR*

From Fig. 5, it can be observed that the magnitude of the *BCR* is highly dependent on the undrained shear strength of the soil. *BCR* is observed to be less than one for all positions and sandy soils when $S_u < 96$ kPa. It is observed that when the position of the clay layer is closer to the footing, the *BCR* varies concavely upwards when the magnitude of S_u is higher. However, this variation is quite minuscule when the internal friction is relatively low. A diverse trend is further noticed, where the *BCR* becomes greater than unity at lower H/B ratios at smaller angles of internal friction, i.e., for $S_u \geq 96$ kPa. This observed behavior can be attributed to the fact that the influence of the clay layer with a higher undrained shear strength dominates over the sand layer with a smaller angle of internal friction. The presence of a clay layer with a higher undrained shear strength provides additional strength to the soil strata.

For $S_u = 192$ kPa, the highest *BCR* is obtained at $H/B = 1$ and the lowest value of *BCR* is obtained at $S_u = 12$ kPa. Throughout the variation of S_u , the bearing capacity ratio of the footing decreases by 37.5 % of its original value when H/B varies between 0.5 to 1 for the sand with internal friction angle, $\phi = 33^\circ$. At the higher ratios of H/B , the value of *BCR* is invariable at 1.0, irrespective of the S_u and ϕ . This supports the notion that beyond a specific depth, the impact of weak clay strata becomes insignificant, and the strength of the strata is not influenced by it. It is worth noting that the internal friction angle plays a distinct role, as it has been observed that a lower friction angle of the sand layer leads to a higher *BCR* for

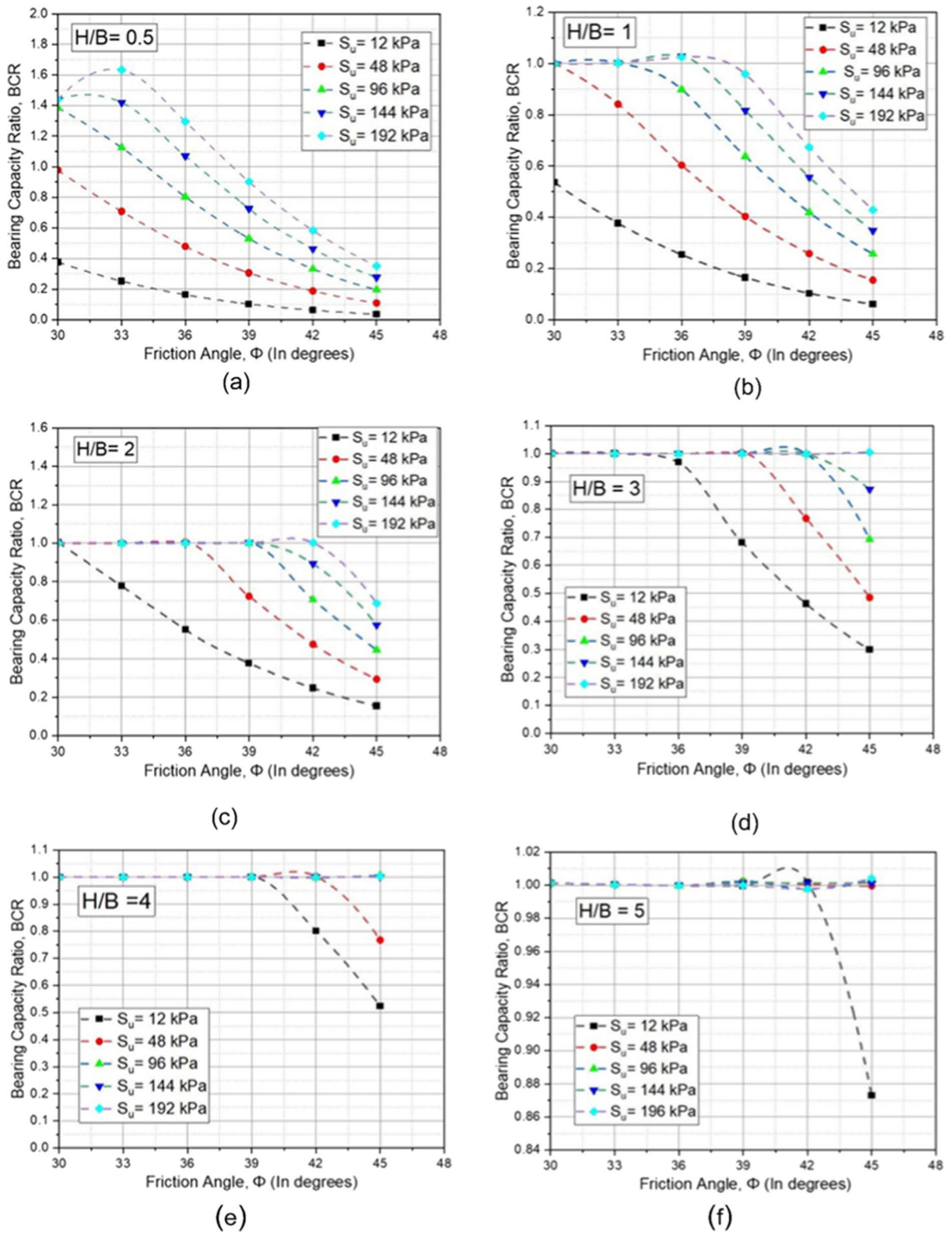


Fig. 4 BCR vs ϕ at varied H/B for a compressible layer having different undrained shear strength and friction angle

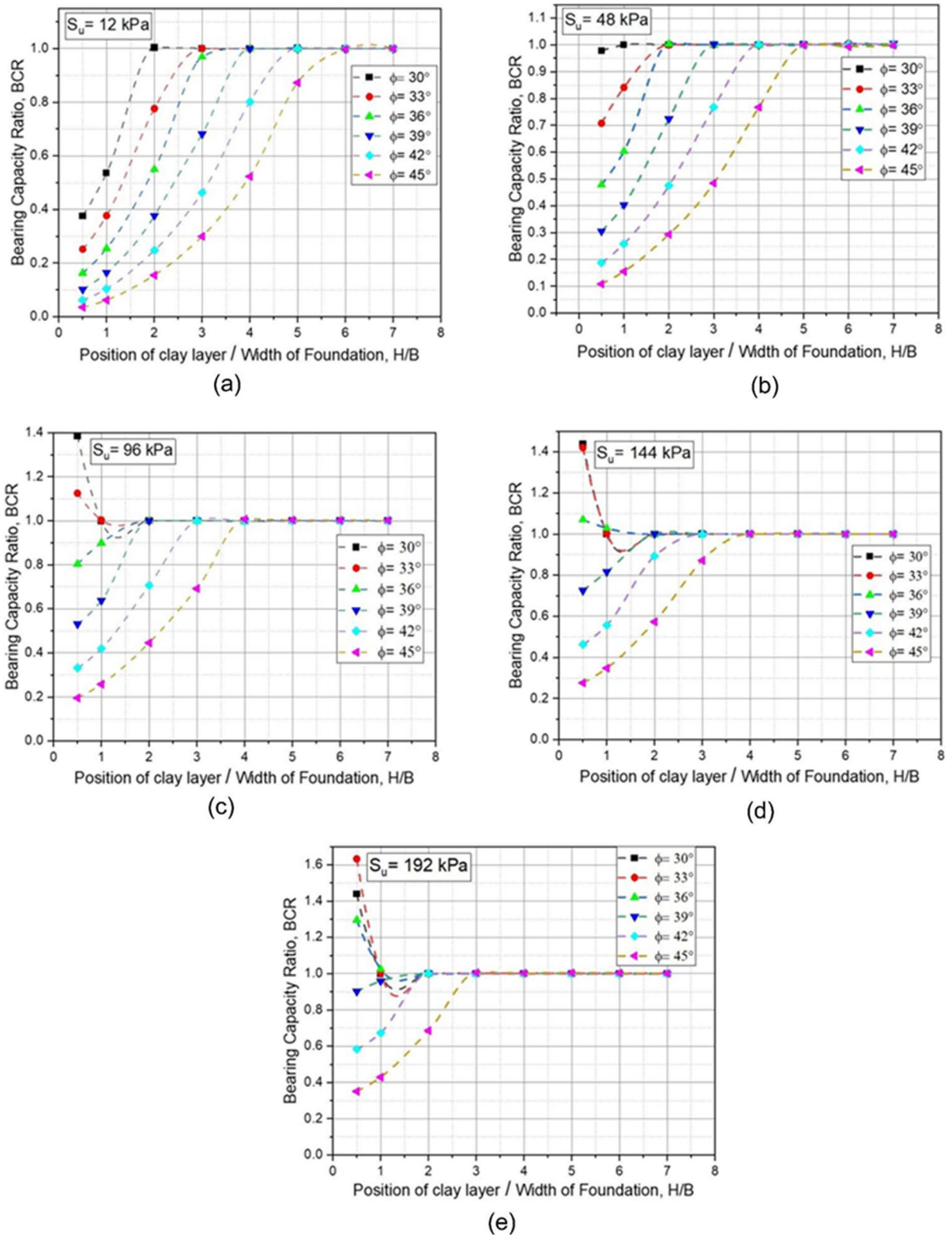
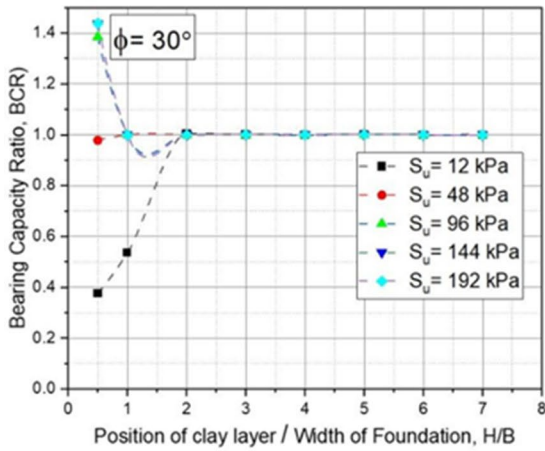
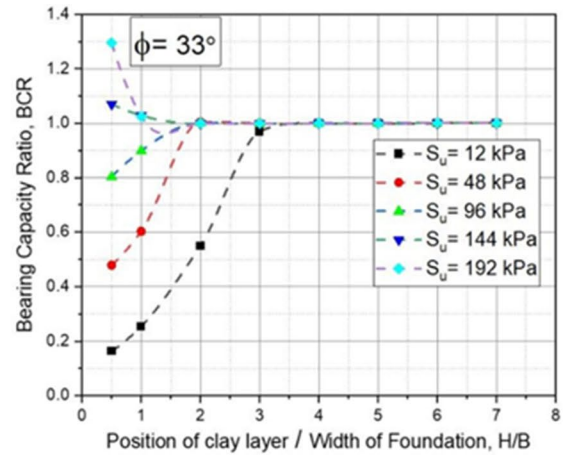


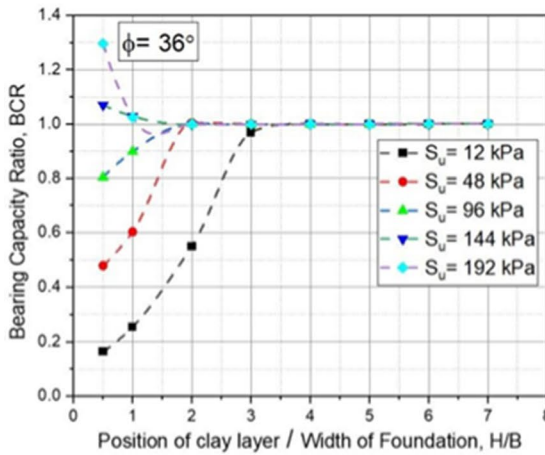
Fig. 5 BCR vs H/B at varied ϕ for different soil strata at different H/B ratios



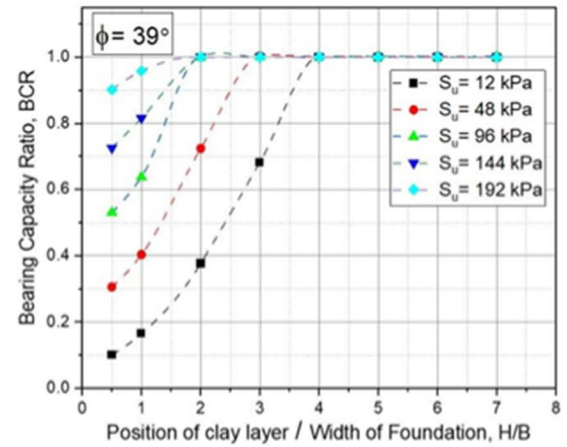
(a)



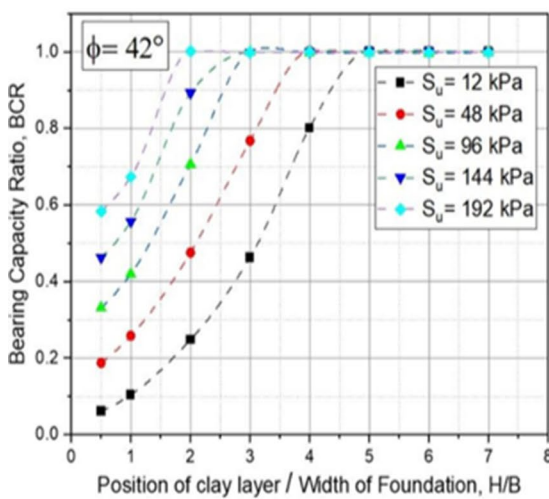
(b)



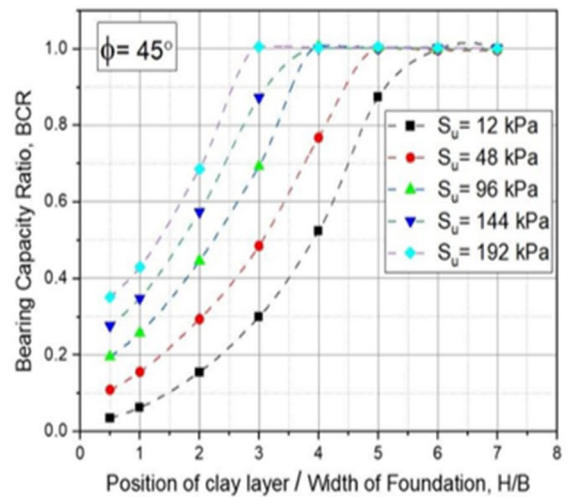
(c)



(d)



(e)



(f)

◀**Fig. 6** *BCR* vs *H/B* at varied S_u for particular soil strata

all S_u and ϕ variations. The *BCR* decreases by 75% from its maximum value with the variation of ϕ .

3.3 Effect of ϕ on *BCR*

Figure 6 shows the variation of *BCR* for varying ϕ for the considered range of *H/B* and S_u . For a constant value of the angle of internal friction ϕ , at particular S_u , the *BCR* increases with an increase in *H/B* ratio and tends to achieve unity at a certain *H/B* ratio. If the clay layer having a greater undrained shear strength is taken into consideration, then the *BCR* decreases with an increase in the *H/B* ratio and tends to reach unity. On increasing the dry density of sand i.e., increasing ϕ , the curve representing the magnitude of the *BCR* changes its course from an upward trend to a downward trend. At the lowest magnitude of ϕ , the *BCR* is constant except for the $H/B \leq 2$. However, as the ϕ increases, more deviation from the constant value of *BCR* are noted at different *H/B* ratios and S_u as depicted in Fig. 5. For loose to medium dense sand strata, i.e., $\phi \leq 36^\circ$, *BCR* is noted to be higher than unity when the clay layer having $S_u \geq 96$ kPa is located $H/B \leq 1$. Additionally, when the internal friction angle of soil strata increases (i.e., $\phi \geq 39^\circ$), the *BCR* is consistently less than unity with the presence of a clay layer, regardless of its location or the undrained shear strength of the clay layer. This observation highlights the fact that the inclusion of clay between a medium-dense sand layer reduces the bearing capacity of the foundation relative to soil strata without clay, regardless of the clay layer's location or undrained shear strength.

3.4 Load-Settlement Behaviour

This section discusses a few typical load settlement curves obtained from the elastoplastic analysis to assist in analyzing the load-carrying capacity and the consequent settlement of the strip footing.

To study the effect of the variation of the position of a clay layer on bearing capacity, the variation of the load-settlement curve for $S_u = 48$ kPa and $\phi = 36^\circ$ is shown in Fig. 7. It has been observed that when soil strata consist solely of sand, the settlement of the footing is substantial, and its bearing capacity

is correspondingly high. However, when a clay layer is interposed in the soil strata, the behavior of the load-settlement curve undergoes a significant change when *H/B* values are equal to 0.5 and 0.1, with the footing experiencing failure at a significantly lower load compared to the scenario of sand-only soil strata. The observed behavior is a result of the presence of a compressible clay layer at shallow depth, leading to failure at a comparatively lower load-carrying capacity (approximately 30–60% lower than the case with no clay). As *H/B* increases, the load-settlement behavior takes on a shape similar to the case soil strata consisting solely of sand. Interestingly, the ultimate load of the footing with $H/B = 2.0$ was found to be slightly higher than the case with no clay. However, a further increase in the distance of the clay layer from the footing results in a decrease in the ultimate failure load. Based on this observed behavior, it can be deduced that there is a critical depth at which the presence of a clay layer with a specific undrained shear strength may enhance the load-bearing capacity of the footing compared to soil strata consisting solely of sand. The location of this critical depth, however, depends on the interaction between sand and clay strengths.

3.4.1 For $H/B = 4$ and $\phi = 36$

In order to study the effect of the undrained shear strength on the bearing capacity of the footing, the variation of the load-settlement curve for $H/B = 4$ and $\phi = 36^\circ$ is shown in Fig. 8. The load settlement curve is not affected by the clay's stiffness, represented by its undrained shear strength, except for very soft clay with a low undrained shear strength of 12 kPa. However, the maximum load-bearing capacity and the settlement at failure are almost the same for all the clays (S_u) considered in the present study. Therefore, for $H/B = 4$, it can be concluded that parameters like ϕ and S_u have no noticeable impact on settlement and load-bearing capacity. This is likely due to the dominance of sand over clay, which negates the effect.

3.4.2 For $H/B = 4$ and $S_u = 48$ kPa

To study the effect of the internal friction of angle on the behavior of the load-settlement curve, a variation of load-settlement for $S_u = 48$ kPa and $H/B = 4$ for ϕ ranging from 30° to 45° is shown in Fig. 9.

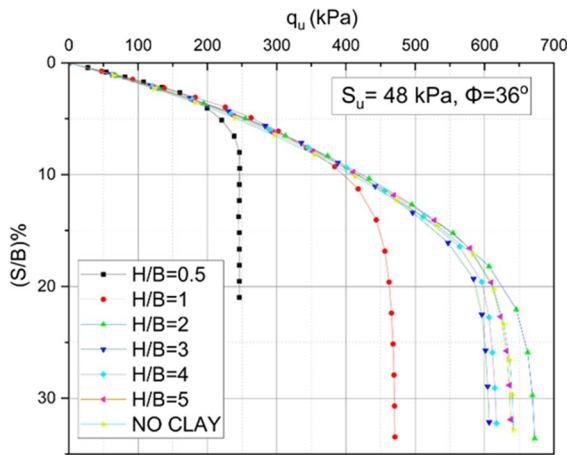


Fig. 7 Load-settlement curve for $\phi = 36^\circ$ and $S_u = 48$ kPa

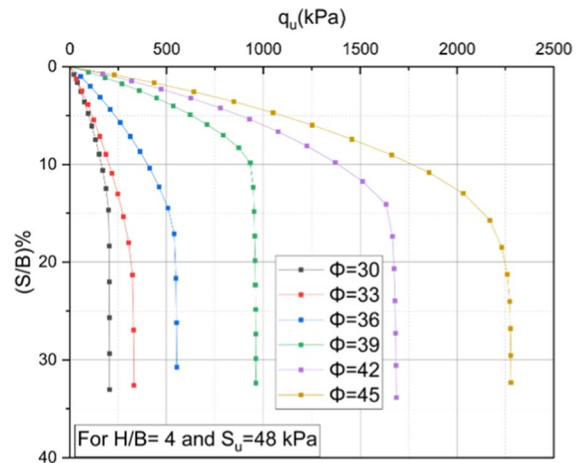


Fig. 9 Load-settlement curve for $S_u = 48$ kPa and $H/B = 4$

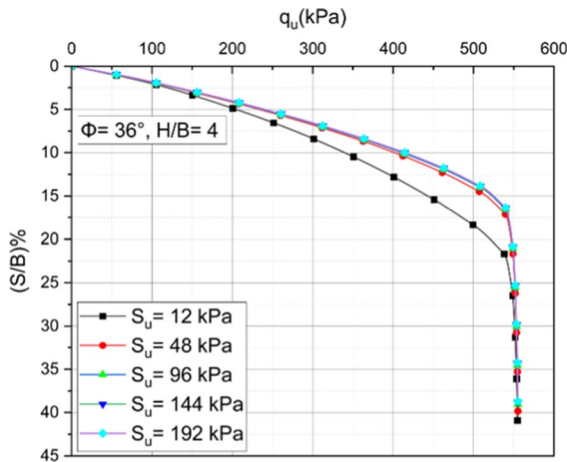


Fig. 8 Load-settlement curve for $\phi = 36^\circ$ and $H/B = 4$

The results of the analysis indicate that an increase in the value of ϕ leads to an improvement in the soil strata’s load-bearing capacity, even when a clay layer is present. This behavior is likely due to the presence of the clay layer at a depth of $H/B = 4$, which does not significantly impact the footing’s settlement behavior under increasing loads. However, it should be noted that the differences in settlement values at failure are not substantial.

The results show that as ϕ increases, the footing’s settlement ratio increases by 9.6% from its

initial value (lowest ϕ). This is likely due to the high H/B ratio, which reduces the impact of the clay layer. Additionally, as the internal friction angle increases, there is a distinct change in the load-bearing capacity at the yield point.

3.5 Progression of the Failure Planes

The variation of the failure pattern of the strip footing on the layered soil strata with respect to the changing values of S_u is shown in Fig. 10. The extent of the failure plane reaches up to the mid of the clay layer when S_u is lower in magnitude. The formation of a high-stress zone is noted at the boundary of the footing which follows a symmetrical pattern at each end. The failure path follows a triangular wedge at both ends that coincide in the center at the clay layer and extends upwards again towards the sand layer. However, with an increment in the values of S_u , it is noted that the extent of the failure plane below the footing is reduced. An interesting fact is also noteworthy that the extent of the failure plane surrounding the footing depends on the undrained shear strength of the clay layer, i.e., the widest failure plane is observed at lowest $S_u = 12$ kPa and the smallest failure plane is obtained when a clay layer has a maximum magnitude of the undrained strength, i.e., $S_u = 192$ kPa.

Figure 11 illustrates the failure path observed at $H/B = 0.5$ and $S_u = 48$ kPa, where the clay layer is closest to the footing among the simulations conducted in this study. The variation in ϕ has a

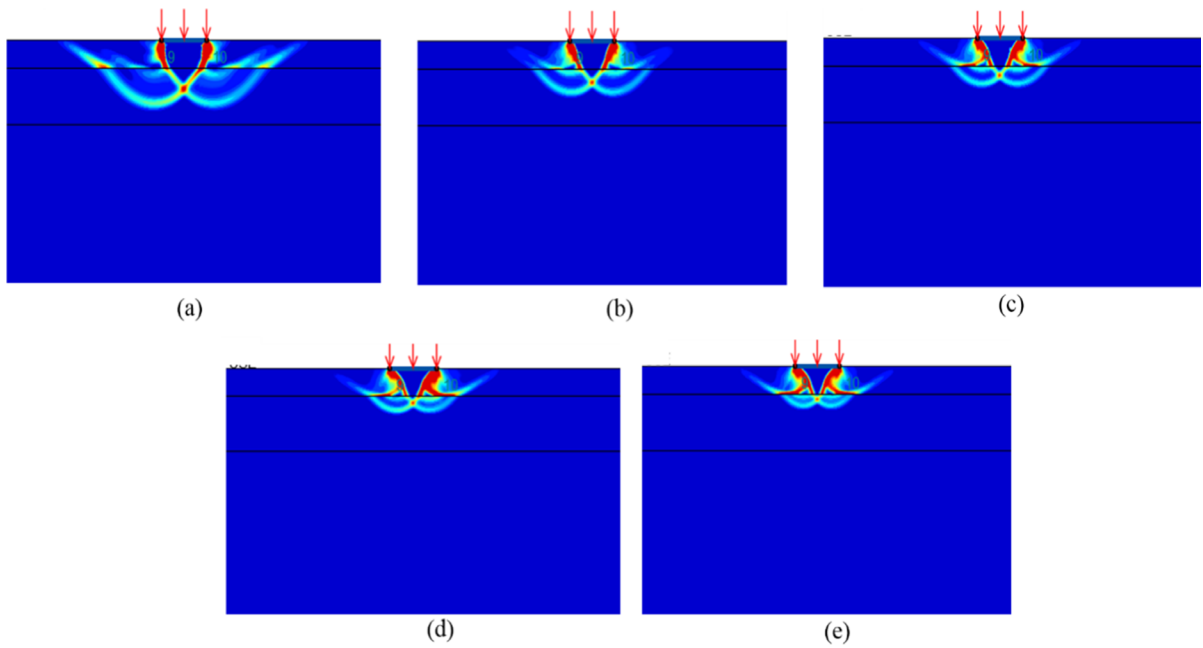


Fig. 10 Failure pattern of soil strata ($\phi = 36^\circ$) having a clay layer at $H/B = 0.5$ with varying undrained shear strength; (a) $S_u = 12$ kPa; (b) $S_u = 48$ kPa; (c) $S_u = 96$ kPa; (d) $S_u = 144$ kPa; and (e) $S_u = 192$ kPa

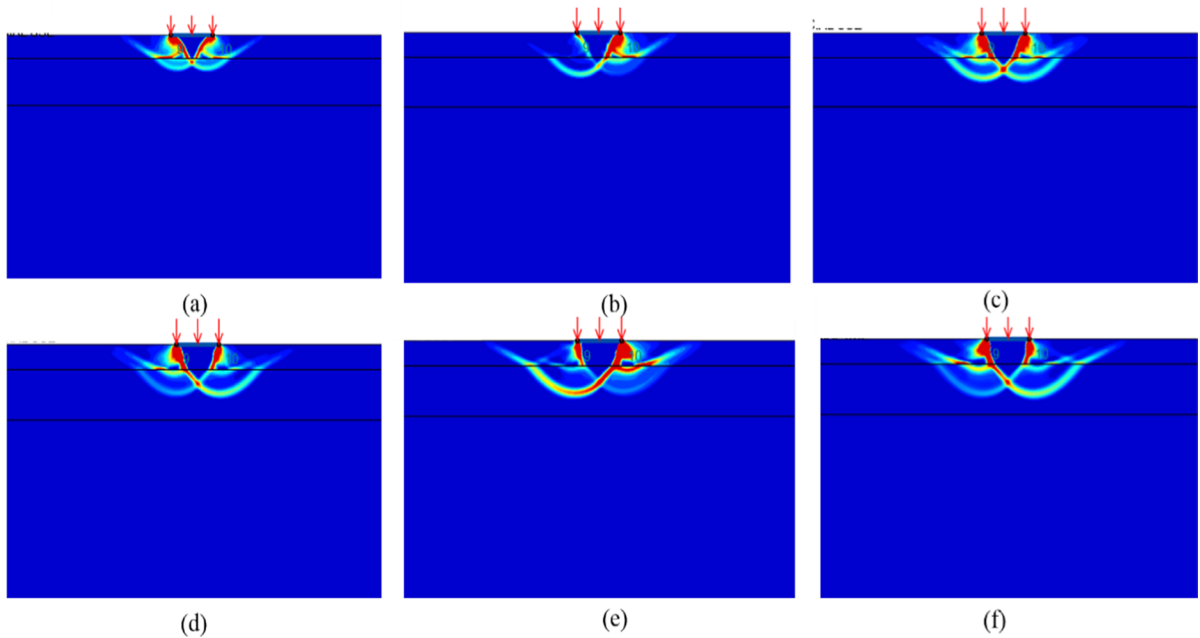


Fig. 11 Failure pattern of a footing resting over cohesionless soil strata with the presence of a clay layer ($S_u = 48$ kPa) at $H/B = 0.5$ for different internal friction angle (ϕ) of (a) $\phi = 30^\circ$; (b) $\phi = 33^\circ$; (c) $\phi = 36^\circ$; (d) $\phi = 39^\circ$ (e) $\phi = 42^\circ$; and (f) $\phi = 45^\circ$

significant impact on the failure plane's path. As the ϕ increases, the extent and depth of the failure plane also increase, encompassing a larger area below the footing. A higher stress zone is noted below the ends of the footing, with the intensity of the stress zone becoming stronger as ϕ increases. The largest failure plane is observed when $\phi = 45^\circ$, and the lowest magnitude is seen when $\phi = 30^\circ$.

Figure 12 depicts the variation in the failure planes as the H/B ratio is changed from 0.5 to 7. The position of the clay layer can be seen to affect the formation of the failure plane beneath the strip footing. When the clay layer is positioned at $H/B = 0.5$, the formation of the failure plane begins below the footing with high-stress zones towards the end, but it is small and somewhat obstructed by the presence of the clay layer. As the H/B ratio increases up to 7, the

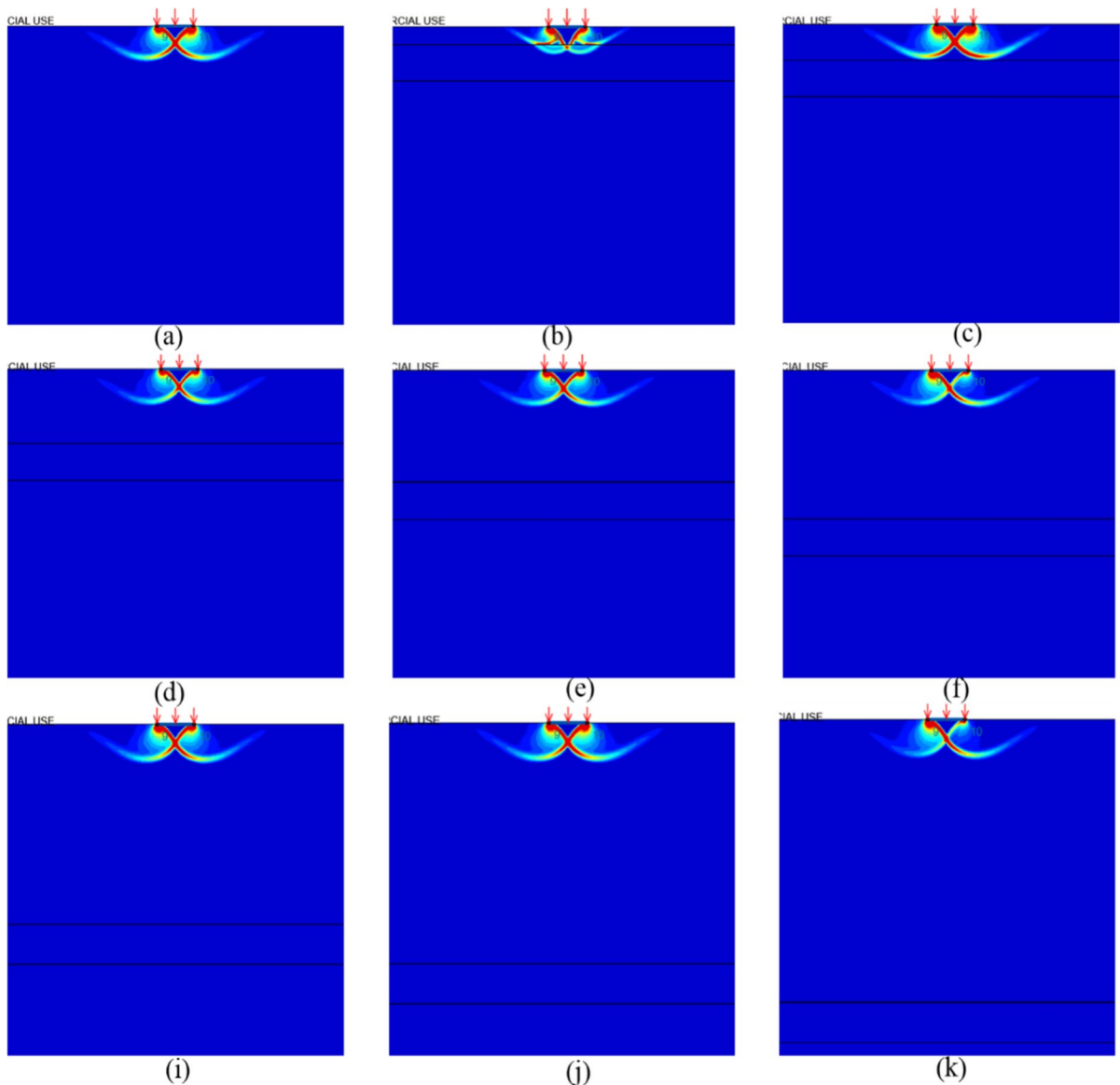


Fig. 12 Failure pattern of cohesionless soil ($\phi = 30^\circ$) with a presence of clay layer ($S_u = 48$ kPa) at a normalized depth of (a) $H/B = 0$ (NO CLAY); (b) $H/B = 0.5$; (c) $H/B = 1$; (d) $H/B = 2$; (e) $H/B = 3$ (f) $H/B = 4$; (g) $H/B = 5$; (h) $H/B = 6$; (i) $H/B = 7$

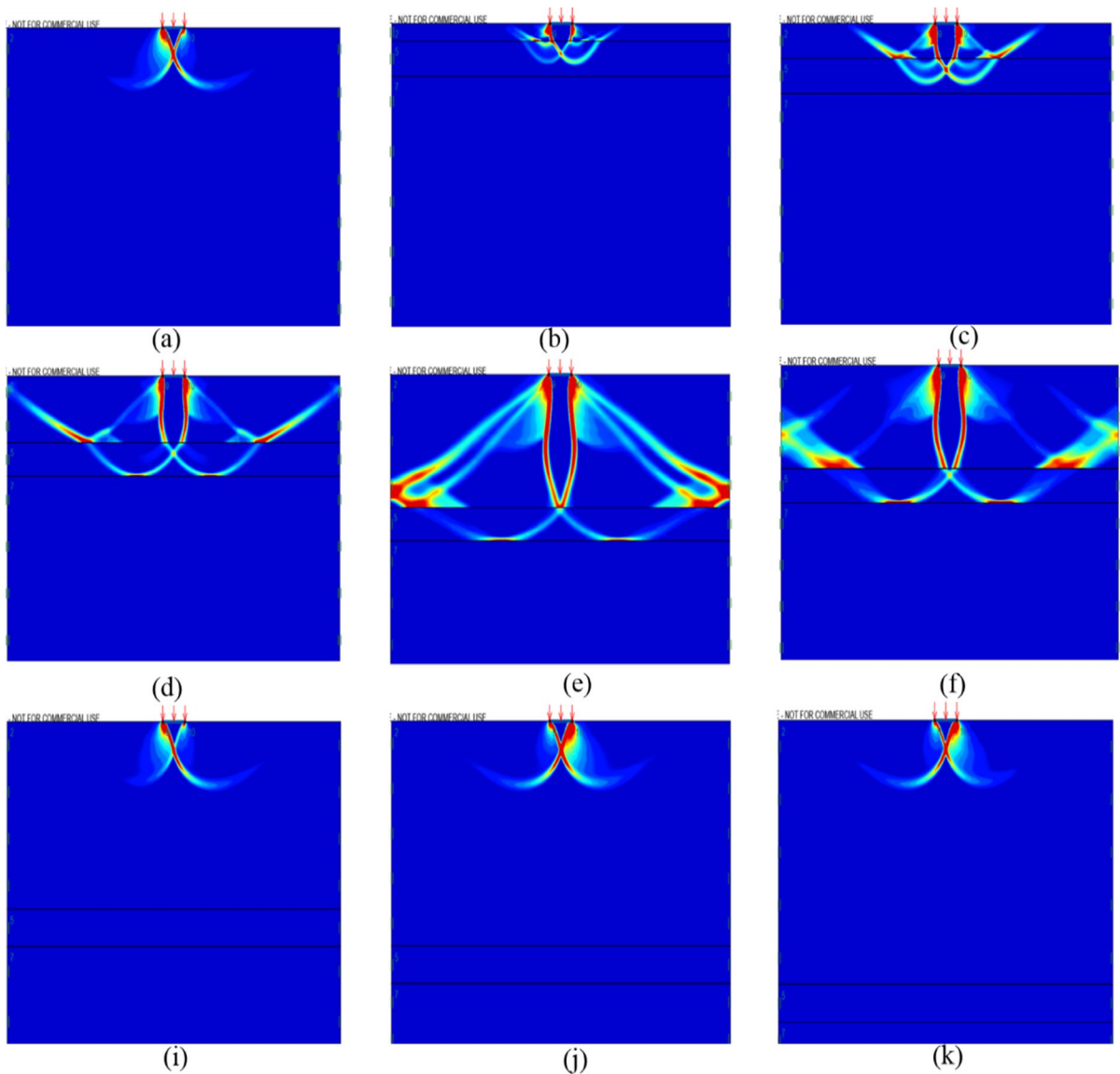


Fig. 13 Failure pattern for varied H/B ratios at $\phi = 45^\circ$ and $S_u = 48$ kPa with the presence of clay layer at a normalized depth of (a) $H/B = 0$ (NO CLAY); (b) $H/B = 0.5$; (c) $H/B = 1$; (d) $H/B = 2$; (e) $H/B = 3$ (f) $H/B = 4$; (g) $H/B = 5$; (h) $H/B = 6$; and (i) $H/B = 7$

magnitude of the failure increases, becoming more pronounced. The high-stress zones are also extended, and two similar wedges converge at the center. It can be concluded that the clay layer does not facilitate the full development of the failure zone.

Figure 13 represents the variation of the failure plane due to varied H/B ratios at constant $\phi = 45^\circ$ and $S_u = 48$ kPa. As the maximum value of ϕ (very dense) is considered in the present study, hence

this particular configuration displays some interesting insights. When there is no clay layer in the considered soil strata, high-stress zones occur beneath the strip footings, proceed in the form of wedges, and further coincide with each other. At this high value of ϕ and clay layer at $H/B = 2$ to 4, the failure planes are not obstructed due to the presence of the clay layer instead they proceed into it. Although the presence of the clay layer is at a certain vertical distance yet it is noticed that the lower stress zones

extend up to a higher depth and a similar coinciding of identical wedge formation happens. For $H/B = 5$ and 6 , the clay layer does not affect the failure plane, and a similar pattern as mentioned before for the progression and coinciding is observed.

4 Sensitivity Analysis, Empirical Formula, and Relative Importance Index from MARS Model

Each input parameter in the initial design of the numerical model is significant since it can be applied in further design optimization of the model. Furthermore, using the empirical equation instead of the numerical model can reduce the cost and time for practical engineering. Hence, the Multivariate Adaptive Regression Spline (MARS) model is adopted in this study for sensitivity analysis and to establish an empirical equation.

MARS model is also identified as an auto mesh regression model. It transfers the complex non-linear regression to a multiple linear regression model, as shown in Fig. 14. MARS progress contains two main steps. Firstly, they procedure a number of linear regression models which are mathematically presented by linear basic functions as shown in Equation (2). Two regression lines are connected by Knot. The position of Knot is determined using the adaptive regression algorithm. In the later step, MARS deletes the least effective linear regression models by using a pruning algorithm based

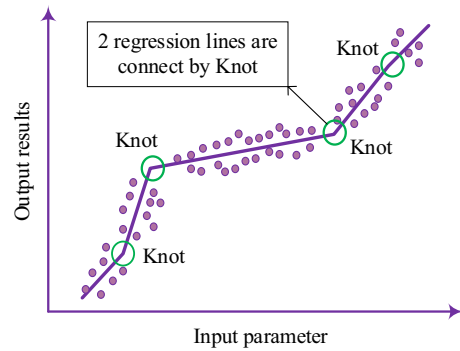


Fig. 14 The idea of the MARS model

on Generalized Cross validation (GCV) (Shiau and Keawsawasvong 2022). The value of GCV can be determined by Equation (3)

$$BF = \max(0, x - t) = \begin{cases} x - t & \text{if } x \geq t \\ 0 & \text{otherwise} \end{cases} \quad (2)$$

where t is a Knot value and x is an input variable

$$GCV = \frac{RMSE}{[1 - (N - hN)/R]^2} \quad (3)$$

where $RMSE$ is the root mean square error for the training dataset, h is the penalty factor, and R is the number of data points.

To build the empirical equation describing the relationship between the input and output parameters, the MARS model merges all linear basic functions (BFs).

Table 1 Basic functions from the optimal model

BF	Equation	BF	Equation	BF	Equation
BF1	Max (0, PHI-39)	BF15	Max (0, H_B-0.5)	BF31	Max (0, PHI-33) × BF29
BF2	Max (0, 39-PHI)	BF16	Max (0, 0.5-H_B)	BF33	Max (0, SU-48) × BF29
BF3	Max (0, H_B-0.5) × BF1	BF17	Max (0, PHI-42) × BF15	BF35	Max (0, SU-12) × BF2
BF4	Max (0, 0.5-H_B) × BF1	BF18	Max (0, 42-PHI) × BF15	BF37	Max (0, 1-H_B) × BF35
BF5	Max (0, SU-96) × BF1	BF19	Max (0, PHI-42) × BF16	BF38	Max (0, H_B-0.5) × BF24
BF6	Max (0, 96-SU) × BF1	BF21	Max (0, PHI-36)	BF39	Max (0, 0.5-H_B) × BF24
BF7	Max (0, H_B-3) × BF5	BF23	Max (0, SU-48)	BF40	Max (0, PHI-33) × BF15
BF8	Max (0, 3-H_B) × BF5	BF24	Max (0, 48-SU)	BF42	Max (0, SU-12) × BF17
BF9	Max (0, H_B-5) × BF1	BF25	Max (0, H_B-0.5) × BF23	BF43	Max (0, PHI-42) × BF29
BF11	Max (0, H_B-1) × BF6	BF26	Max (0, 0.5-H_B) × BF23	BF45	Max (0, SU-12) × BF43
BF12	Max (0, 1-H_B) × BF6	BF27	Max (0, H_B-3) × BF6	BF46	Max (0, H_B-0.5) × BF35
BF13	Max (0, SU-96) × BF9	BF29	Max (0, H_B-3)	BF48	Max (0, PHI-33) × BF16
BF14	Max (0, 96-SU) × BF9				

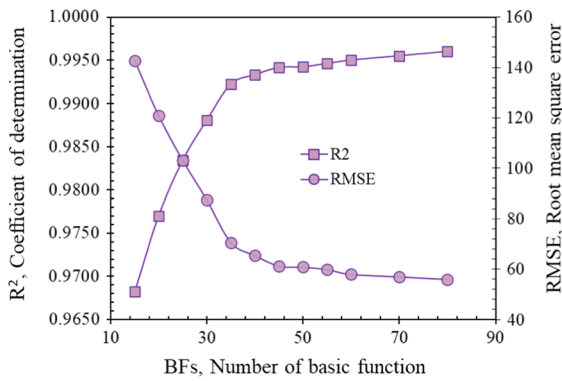


Fig. 15 Influence of variation of BF on the accuracy of MARS models

The form of n^{th} equation is shown in Eq. (4), where a_0 is a constant, N is the number of BFs , g_n is the n^{th} BF , a_n is the n^{th} coefficient of g_n . Note that increasing the number of data sections, in other words, the number of basic functions, can increase the accuracy of the MARS model (Yodsomjai et al. 2022; Jearsiripongkul et al. 2022; Sirimontree et al. 2022).

$$f(x) = a_0 + \sum_{n=1}^N a_n g_n(X) \tag{4}$$

In this study, all numerical results are used as the training data for MARS model. In detail, the data set includes 210 UBC values from numerical analysis corresponding with 210 datasets of input dimensionless parameters (H/B , ϕ , S_u). The optimal model is selected by considering the variation of two classical statistical standards, i.e., Root Mean Squared Error ($RMSE$) and coefficient of determination (R^2) due to the changing of the number of basic functions. In that, the R^2 is in the range of 0 to 1. The R^2 close to 1 indicates that the exact agreement between prediction from MARS model and the target value is obtained while R^2 close to 0 is inverse meaning. $RMSE$ is used to determine errors between prediction and target value. $RMSE$ value is smaller which shows a model with higher accuracy.

As results shown in Fig. 15, it can be seen that the $RMSE$ and R^2 are changed due to the variation of the number of basic functions. $RMSE$ reduces while R^2 is closed to 1 when the number of basic functions rises. The variations of $RMSE$ and R^2 become stable when the number of basic functions is 50. So, MARS model

with 50 basic functions is used for the next analysis. The basic functions of the optimal MARS model are shown in Table 1.

Figure 16 shows the comparison between UBC determined from the proposed empirical equation and numerical results. It can be seen that UBC values from the proposed equation are in well agreement with those from numerical results with a high R^2 of 99.42%. This means that the proposed equation can be a useful tool for practical engineering to predict the UBC as well as the bearing capacity of layered soil with an interbedded weak clay layer. The proposed empirical equation is shown in Eq. 5.

$$\begin{aligned}
 UBC = & 279.251 + 41.6155 \times BF3 + 251.365 \times BF4 + 0.753529 \times \\
 & BF5 - 0.780422 \times BF6 - 0.608465 \\
 & \times BF7 - 0.264262 \times BF8 - 83.7718 \times \\
 & BF9 - 0.619037 \times BF11 + 1.01617 \times BF12 \\
 & + 0.897852 \times BF13 - 0.505036 \times \\
 & BF14 + 100.665 \\
 & \times BF15 - 6.56242 \times BF18 + 429.443 \times BF19 + 12.9417 \times \\
 & BF21 + 3.48765 \times BF23 - 5.95136 \times BF24 \\
 & - 1.16095 \times BF25 - 5.77517 \times \\
 & BF26 + 1.38747 \times BF27 - 72.9691 \times BF29 \\
 & - 21.3214 \times BF31 + 0.912378 \times \\
 & BF33 - 0.360997 \times BF350.243619 \times BF37 \\
 & + 1.04753 \times BF38 + 10.8786 \times \\
 & BF39 + 22.0313 \times BF40 + 0.320371 \times BF42 \\
 & + 71.312 \times BF43 - 0.509995 \times \\
 & BF45 + 0.0701428 \times BF46 + 178.711 \times BF48
 \end{aligned} \tag{5}$$

The MARS model employs the relative important index (RII) to assess the significance of each parameter. RII is computed based on the difference in the generalized cross-validation (GCV) values between the pruned and over-fitted versions of the model (as described in Gan et al. 2014 and Steinberg et al. 1999). The score relative importance index (RII) is determined by Eq. 6:

$$RII(i) = \frac{\Delta g(i)}{\max \{ \Delta g(i), \Delta g(2), \Delta g(3), \dots, \Delta g(n) \}} \tag{6}$$

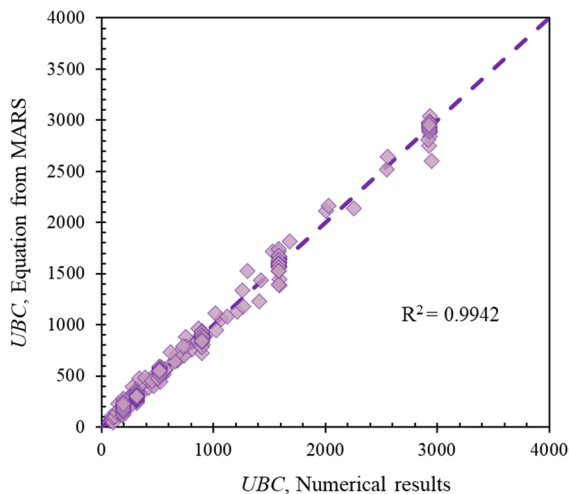


Fig. 16 Comparison between proposed empirical equation and numerical results

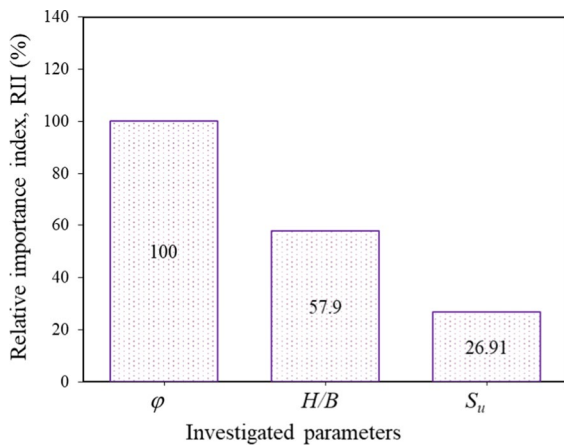


Fig. 17 Relative important index of the dimensionless parameters

where Δg is the increase in GCV when i^{th} parameter is deleted. The higher the GCV rises, the more significant the deleted parameter.

The results of the sensitivity analysis are obtained in Fig. 17. It is noted that RII of 100% means that the corresponding parameters in the most important ones. As a result, ϕ is the most important parameter while H/B and S_u are scored later with RII values of 57.9% and 26.91%, respectively. These results signify that the three investigated dimensionless parameters are highly essential and cannot be neglected in

determining the bearing capacity of layered soil with an interbedded weak clay layer.

5 Conclusions

The present study aims to investigate the impact of a compressible clay layer situated within soil strata on the ultimate bearing capacity of a strip footing. The depth of the compressible layer (H/B) and the internal angle of friction of sand (ϕ) as well as the undrained shear strength of the clay layer (S_u) are varied. A finite element analysis is carried out to assess the bearing capacity ratio (BCR). The numerical model underwent limit and elastoplastic analysis and the shear failure patterns beneath the footing are analyzed. The Multivariate Adaptive Regression Spline ($MARS$) model is employed to develop a correlation equation that portrays the non-linearities and interactions between variables. The results are compared to numerical and empirical data, and the RII of the parameters is evaluated.

1. The outcomes from the study shows that when the compressible clay layer is located close to the footing ($H/B = 0.5$), the BCR is proportional to the undrained shear strength of the clay layer. The highest BCR is obtained at $S_u = 192$ kPa and the lowest BCR is obtained at $S_u = 12$ kPa. The BCR is also proportional to S_u when the compressible layer is close to the foundation. The highest BCR is obtained when the clay layer is situated between sandy soil with a lower friction angle ($\phi = 33^\circ$) and the minimum is obtained when the sandy soil had a higher friction angle ($\phi = 45^\circ$). However, for higher $H/B = 4$ and 5, no effect of undrained shear strength and internal friction angle is observed, and the BCR is noted to be constant at 1.0.
2. The study also found that the magnitude of the BCR is highly dependent on the undrained shear strength of the soil. The BCR became greater than unity at lower H/B ratios and lower internal friction angles, which might be due to the clay layer with a higher undrained shear strength overpowering the sand layer with a smaller internal friction angle. The impact of the horizontal clay layer on the load-carrying capacity diminished as the H/B ratio increased.

3. The study concluded that the development of the failure envelope below the footing was governed by the location of the clay layer and the relative stiffness between the sand and clay layer.
4. The *MARS* model is used to propose an empirical equation for determining the bearing capacity of layered soil with an interbedded weak clay layer, with an R^2 value of 99.42. The internal friction angle (ϕ) is found to be the most important input parameter with $R_{II} = 100$, while H/B and S_u have R_{II} values of 57.9% and 26.91%, respectively.

6 Declaration

Acknowledgements We acknowledge Ho Chi Minh City University of Technology (HCMUT), VNU–HCM for supporting this study.

Funding This research did not receive any specific grant from funding agencies in the public, commercial, or not-for-profit sectors.

Data availability All the data associated with the study are present in the manuscript itself.

Declarations

Conflict of interest On behalf of all authors, the corresponding author states that there is no conflict of interest.

References

- Akinmusuru JO, Akinbolade JA (1981) Stability of loaded footings on reinforced soil. *J Geotech Eng Division* 107(6):19–827
- Ameratunga J, Sivakugan N, Das BM (2016) *Correlations of soil and rock properties in geotechnical engineering*.
- Banyong R, Keawsawasvong S (2022) Stability of limiting pressure behind soil gaps in contiguous pile walls in anisotropic clays. *Eng Fail Anal* 134:106049
- Chakraborty D, Kumar J (2014) Bearing capacity of strip foundations in reinforced soils. *Int J Geomech* 14(1):45–58
- Chakraborty M, Kumar J (2014) Bearing capacity of circular foundations reinforced with geogrid sheets. *Soils Found* 54(4):820–832
- Chauhan VB, Srivastava A, Jaiswal S, Keawsawasvong S (2022) Behavior of back-to-back MSE walls: interaction analysis using finite element modeling. *Transp Infrastruct Geotechnol* 1–25.
- Cicek E, Guler E (2015) Bearing capacity of strip footing on reinforced layered granular soils. *J Civil Eng Manag* 21(5):605–614
- Dewaikar DM, Mohapatra BG (2003) Computation of bearing capacity factor N_γ -Prandtl's mechanism. *Soils Found* 43(3):1–10
- Fragaszy RJ, Lawton E (1984) Bearing capacity of reinforced sand subgrades. *J Geotech Eng* 110(10):1500–1507
- Gan Y, Duan Q, Gong W, Tong C, Sun Y, Chu W, Ye A, Miao C, Di Z (2014) A comprehensive evaluation of various sensitivity analysis methods: a case study with a hydrological model. *Environ Model Softw* 51:269–285
- Ghazavi M, Eghbali AH (2008) A simple limit equilibrium approach for calculation of ultimate bearing capacity of shallow foundations on two-layered granular soils. *Geotech Geol Eng* 26(5):535–542
- Gupta A, Chauhan VB, Patel V (2021) Uttar Pradesh. CRC Press, In *Geotechnical Characteristics of Soils and Rocks of India*, pp 671–693
- Hanna AM (1987) Finite element analysis of footings on layered soils. *Math Model* 9(11):813–819
- Hanna AM, Meyerhof GG (1980) Design charts for ultimate bearing capacity of foundations on sand overlying soft clay. *Can Geotech J* 17(2):300–303
- Jaiswal S, Chauhan VB (2021) Assessment of seismic bearing capacity of a strip footing resting on reinforced earth bed using pseudo-static analysis. *Civil Environ Eng Rep* 31(2):117–137
- Jaiswal S, Chauhan VB (2021) Response of strip footing resting on earth bed reinforced with geotextile with wrap-around ends using finite element analysis. *Innov Infrastruct Solut* 6:121
- Jaiswal S, Chauhan VB (2021) Evaluation of optimal design parameters of the geogrid reinforced foundation with wrap-around ends using adaptive FEM. *Int J Geosynth Ground Eng* 7(4):77
- Jaiswal S, Srivastava A, Chauhan VB (2022) Numerical modeling of soil-nailed slope using drucker-prager model. *Advances in geo-science and geo-structures*. Springer, Singapore, pp 97–105
- Jaiswal S, Chauhan VB (2021b) Ultimate bearing capacity of strip footing resting on rock mass using adaptive finite element method. *J King Saud Univ-Eng Sci*.
- Jaiswal S, Srivastava A, Chauhan VB (2022a) Performance of strip footing on sand bed reinforced with multilayer geotextile with wrap-around ends. In: *Ground Improvement and Reinforced Soil Structures: Proceedings of Indian Geotechnical Conference 2020 Volume 2*, Springer, Singapore, pp. 721–732.
- Jaiswal S, Srivastava A, Chauhan VB (2021) Improvement of bearing capacity of shallow foundation resting on wrap-around geotextile reinforced soil. In: *International Foundations Congress and Equipment Expo 2021*. ASCE, GSP 324, Dallas, Texas, pp. 65–74.
- Jearsiripongkul T, Lai VQ, Keawsawasvong S, Nguyen TS, Van CN, Thongchom C, Nuaklong P (2022) Prediction of uplift capacity of cylindrical caissons in anisotropic and inhomogeneous clays using multivariate adaptive regression splines. *Sustainability* 14(8):4456
- Keawsawasvong S, Lai VQ (2021) End bearing capacity factor for annular foundations embedded in clay considering the effect of the adhesion factor. *Int J Geosynth Ground Eng* 7(1):1–10
- Keawsawasvong S, Ukritchon B (2019) Undrained basal stability of braced circular excavations in non-homogeneous clays with linear increase of strength with depth. *Comput Geotech* 115:103180

- Keawsawasvong S, Ukritchon B (2020) Failure modes of laterally loaded piles under combined horizontal load and moment considering overburden stress factors. *Geotech Geol Eng* 38:4253–4267
- Keawsawasvong S, Shiau J, Yoonirundorn K (2022) Bearing capacity of cylindrical caissons in cohesive-frictional soils using axisymmetric finite element limit analysis. *Geotech Geol Eng* 40:3913–3928
- Keawsawasvong S, Shiau J, Limpanawannakul K, Panomchaivath S (2022) Stability charts for closely spaced strip footings on Hoek-Brown rock mass. *Geotech Geol Eng* 40:3051–3066
- Keawsawasvong S, Shiau J, Ngamkhanong C, Qui Lai V, Thongchom C (2022) Undrained stability of ring foundations: axisymmetry, anisotropy, and nonhomogeneity. *Int J Geomech* 22(1):04021253
- Kumar J, Chakraborty M (2015) Bearing capacity factors for ring foundations. *J Geotech Geoenviron Eng* 141(10):06015007
- Kumar J, Sahoo JP (2013) Bearing capacity of strip foundations reinforced with geogrid sheets by using upper bound finite-element limit analysis. *Int J Numer Anal Methods Geomech* 37(18):3258–3277
- Lai VQ, Nguyen DK, Banyong R, Keawsawasvong S (2022) Limit analysis solutions for stability factor of unsupported conical slopes in clays with heterogeneity and anisotropy. *Int J Comput Mater Sci Eng* 11(1):2150030–128
- Lai VQ, Shiau J, Keawsawasvong S, Tran DT (2022) Bearing capacity of ring foundations on anisotropic and heterogeneous clays ~ FEA, NGI-ADP, and MARS. *Geotech Geol Eng* 40:3929–3941
- Lai VQ, Banyong R, Keawsawasvong S (2022) Undrained sinkhole collapse in anisotropic clays. *Arab J Geosci* 15(8):1–13
- Mandal JN, Sah HS (1992) Bearing capacity tests on geogrid-reinforced clay. *Geotext Geomembr* 11(3):327–333
- Meyerhof GG (1963) Some recent research on the bearing capacity of foundations. *Can Geotech J* 1(1):16–26
- Meyerhof GG, Hanna AM (1978) Ultimate bearing capacity of foundations on layered soils under inclined load. *Can Geotech J* 15(4):565–572
- Michalowski RL, Shi L (1995) Bearing capacity of footings over two-layer foundation soils. *J Geotech Eng* 121(5):421–428
- Ojha R, Srivastava A, Chauhan VB (2021) Study of geosynthetic reinforced retaining wall under various loading. *Ground Improvement Techniques*. Springer, Singapore, pp 339–351
- Optum G2 (2020) Finite Element Program for Geotechnical Analysis. Optum Computational Engineering, www.optumce.com
- Rai H, Keawsawasvong S, Chavda JT (2022) Numerical investigations on evaluation of undrained stability of active and passive strip, circular, and annular trapdoors. *Geotech Geol Eng* 1–12.
- Shiau JS, Lyamin AV, Sloan SW (2003) Bearing capacity of a sand layer on clay by finite element limit analysis. *Can Geotech J* 40(5):900–915
- Shiau J, Keawsawasvong S (2022) Multivariate adaptive regression splines analysis for 3D slope stability in anisotropic and heterogeneous clay. *J Rock Mech Geotech Eng*
- Sirimontree S, Jearsiripongkul T, Lai VQ, Eskandarinejad A, Lawongkerd J, Seehavong S, Thongchom C, Nuaklong P, Keawsawasvong S (2022) Prediction of penetration resistance of a spherical penetrometer in clay using multivariate adaptive regression splines model. *Sustainability* 14(6):3222
- Sloan SW (2013) Geotechnical stability analysis. *Géotechnique* 63(7):531–572
- Srinivasa Murthy BR, Sridharan A, Singhhy HR (1993) Analysis of reinforced soil beds. *Indian Geotech J* 23(4):447–458
- Srivastava A, Chauhan VB (2020) Numerical studies on two-tiered MSE walls under seismic loading. *SN Appl Sci* 2(10):1–7
- Steinberg D, Colla PL, Martin K (1999) MARS user guide. San Diego, CA: Salford Systems.
- Terzaghi K (1943) Theoretical soil mechanics. Chapman and Hall, London
- Ukritchon B, Keawsawasvong S (2019) Design equations of uplift capacity of circular piles in sands. *Appl Ocean Res* 90:101844
- Ukritchon B, Keawsawasvong S (2020) Undrained stability of unlined square tunnels in clays with linearly increasing anisotropic shear strength. *Geotech Geol Eng* 38(1):897–915
- Ukritchon B, Yoang S, Keawsawasvong S (2019) Three-dimensional stability analysis of the collapse pressure on flexible pavements over rectangular trapdoors. *Transp Geotech* 21:100277
- Ukritchon B, Yoang S, Keawsawasvong S (2020) Undrained stability of unsupported rectangular excavations in non-homogeneous clays. *Comput Geotech* 117:103281
- Yodsomjai W, Keawsawasvong S, Lai VQ (2021) Limit analysis solutions for bearing capacity of ring foundations on rocks using Hoek-Brown failure criterion. *Int J Geosynth Ground Eng* 7(2):1–10
- Yodsomjai W, Lai VQ, Banyong R, Chauhan VB, Thongchom C, Keawsawasvong S (2022) A machine learning regression approach for predicting basal heave stability of braced excavation in non-homogeneous clay. *Arab J Geosci* 15(9):873

Publisher's Note Springer Nature remains neutral with regard to jurisdictional claims in published maps and institutional affiliations.

Springer Nature or its licensor (e.g. a society or other partner) holds exclusive rights to this article under a publishing agreement with the author(s) or other rightsholder(s); author self-archiving of the accepted manuscript version of this article is solely governed by the terms of such publishing agreement and applicable law.